Supplementary Information

Semi-embedded Ni@ZSM-5 catalyst for efficient fatty acid hydrodeoxygenation: Role of metal–support interaction

Guanyi Zhang,[1,3] Hao Yan,[1] Lei Wang,*[1,3,4] Zhihao Zheng,[1] Dawei Wang,[1] Siyuan Zheng,[1] Zhitong Qian,[1] Luxuan Sun,[1] Haisong Feng,[1] Xin Zhang,[1] Weiming Zhai,*[2] Feng Liu,*[2] Zhihai Hu,[2] and Yusen Yang*[1,3]

[1] State Key Laboratory of Chemical Resource Engineering, Beijing Advanced Innovation Center for Soft Matter Science and Engineering, Beijing University of Chemical Technology, Beijing 100029, P. R. China

[2] SINOPEC Research Institute of Petroleum Processing Co., Ltd., Beijing 100083, P. R. China

[3] Quzhou Institute for Innovation in Resource Chemical Engineering, Quzhou 324000, Zhejiang Province, P. R. China

[4] Chemical Reaction Engineering and Technology, Tsinghua University, Beijing, 100084 China

Author Information

***** Corresponding authors. Tel: +86-10-64412131; Fax: +86-10-64425385.

E-mail addresses: wang-lei@tsinghua.edu.cn (L. Wang); zhaiweiming.ripp@sinopec.com (W. Zhai); liuf.ripp@sinopec.com (F. Liu); yangyusen@mail.buct.edu.cn (Y. Yang).

■ SUPPLEMENTARY SECTION

1. Experimental

1.1 Chemicals and materials

$Ni(NO_3)_2·6H_2O$ (GR, 99%) and sodium acetate (anhydrous) (>99%) were purchased from Macklin Biochemical Co., Ltd. (China). The HZSM-5 zeolites (SiO_2/Al_2O_3 = 25, 85, 200 and 300) were purchased from Nankai University Catalyst Co. Ltd. The reaction substrate including palmitic acid were supplied by Shanghai Macklin Biochemical Co., Ltd. (China). All the reagents and chemicals were used directly without any further purification.

1.2 Synthesis of catalysts

Ni@ZSM-5: The Ni@ZSM-5 catalyst was synthesized by a base-assisted hydrothermal method: Typically, dispersing 0.5 g of the HZSM-5(Si/Al=200) powder into 50 ml of deionized water and carrying out ultrasonic treatment for 0.5 h. Meanwhile, 0.248 g of $Ni(NO_3)_2·6H_2O$ (the content of Ni was 10wt% of HZSM-5) is dissolved in 40 ml of deionized water to form another solution. The nickel salt solution was slowly dropped into the ZSM-5 suspension, followed by the addition of a certain amount of anhydrous sodium acetate solid until complete dissolution, and the pH of the suspension was controlled at 8.5. After thorough stirring, it was transferred to Teflon-lined autoclave and hydrothermally treated at 160 ℃ for 12 h. Under given alkaline conditions, the following reactions occur: $Ni^{2+} + OH^- + SiO_2·nH_2O \rightarrow Ni_3Si_4O_{10}(OH)_2 + nH_2O$. $Ni_3Si_4O_{10}(OH)_2$ is a green solid with a nickel phyllosilicate structure. The greenish solid powder was collected by centrifugal separation and then dried sufficiently in a vacuum dryer for 6 h. Finally, the obtained powder was heated at a ramping rate of 5 °C/min up to 600 °C in tube furnace under a 10% H_2/N_2 (v/v = 1:9) flow and keep for 4 h. In this case, the nickel in the nickel phyllosilicate precursor is reduced in situ to give fine Ni nanoparticles

semi-embedded in the ZSM-5 zeolite support. Followed by cooling down to 50 °C and then to room temperature in nitrogen. The final products were denoted as Ni@ZSM-5.

Ni/ZSM-5: The Ni/ZSM-5 catalyst was prepared via the wet impregnation method. Firstly, HZSM-5(Si/Al=200) were pretreated by calcination in a muffle furnace at 550 ℃ for 4 h with a ramping rate of 5 °C/min. Then HZSM-5 (0.5 g) was dispersed in 30 mL H_2O, followed by a slow dropping of $Ni(NO_3)_2 \cdot 6H_2O$ aqueous solution (the content of Ni was 10wt% of HZSM-5) with magnetic stirring. After 4 h, the solvent was heated to evaporate water at 80 ℃ to acquire the dehydrated sample. The reduction treatment was conducted at 600 ℃ for 4 h in 10% H_2/N_2 (v/v = 1:9) followed by cooling down to 50 °C and then to room temperature in nitrogen, Ni/HZSM-5 was obtained.

1.3 Characterizations

The powder X-ray diffraction (XRD) patterns were performed on a Rigaku XRD-6000 diffractometer using Cu Ka (λ=0.15418 nm) X-ray source (40 kV) with a scanning speed of 5°/min and a scan range of 5−80°. Scanning electron microscope (SEM) measurements were performed on Zeiss Supra 55. Nitrogen adsorption–desorption curves were obtained on a Micromeritics ASAP 2460 instrument with low-temperature N_2 adsorption-desorption. Transmission electron microscope (TEM) and high-resolution transmission electron microscope (HR-TEM) measurements were carried out on a JEOLJEM-2010. X-ray photoelectron spectra (XPS) were obtained on a Thermo VG Escalab 250 X-ray photoelectron spectrometer. X-ray absorption fine structure (XAFS) spectra at the Cu K-edge were recorded in transmission mode at beamlines 1W1B and 1W2B of the Beijing Synchrotron Radiation Facility (BSRF), Institute of High Energy Physics (IHEP), Chinese Academy of Sciences (CAS). Data analysis was carried out using Athena and Artemis in the Ifeffit and Demeter package. For extended

X-ray absorption fine structure (EXAFS) fitting, theoretical scattering paths were generated with FEFF 6.0 L. The k3-weighted EXAFS oscillations were analyzed in the k-range of 2.0–12.0 Å−1, R-range of 1.0–3.0 Å, with an S_0^2 value of 0.73. Raman spectra were recorded on RM1000 spectrometer (532 nm, 50 mW excitation laser). The N_2 sorption analysis was carried out on ASAP-2460 equipment at 77 K from Micromeritics. The pore size distribution plot was recorded from the desorption branch of the isotherm based on the Barrett-Joyner-Halenda (BJH) model. The Ni loading content in catalyst quantitative were measured by inductively coupled plasma-atomic emission spectroscopy (ICP-AES, PerkinElmer instruments, Norwalk, 2l00 DV, USA).

H_2-Temperature-Programmed-Reduction (H_2-TPR) measurements were performed using a TPD/R/O 1100 system (Thermo Scientific) equipped with a thermal conductivity detector (TCD). Before each TPR measurement, a 100 mg catalyst sample was outgassed in Ar at 300 °C for 2 h to remove impurities and then allowed to cool down to room temperature. For the TPR measurements, 50 mL/min of a 5% H_2/N_2 mixture was passed through the catalyst bed while the furnace temperature was increased at a rate of 10 °C min^{-1} from 50 °C to 800 °C. Temperature programmed desorption of NH_3 (NH_3-TPD) was performed on the same instrument as Auto Chem. II2920 (Mircromeritics, USA). Prior to the adsorption of NH_3, 50 mg samples were pretreated with Ar gas at 150 ℃ for 0.5 h to clean surface impurities from moisture and other adsorbed gases. After cooling to 100 ℃, the catalyst was saturated with pure NH_3 and then, purged with He gas to remove the physisorbed NH_3. Subsequently, the sample was heated to 800 ℃ at a heating rate of 10 ℃/min and the NH_3 desorption (m/z = 16) was detected by MS (Agilent). Temperature programmed desorption of hydrogen (H_2-TPD) was performed as follows. 50 mg of sample was pretreated in a pure H_2 (100 mL/min for 2 h at 300 ℃), followed by purging Ar (100 mL/min for 2 h) and then cooling to room temperature. The sample was saturated with

10% H_2/Ar at 50 ℃ and then purged with Ar at the same temperature for 1 h to remove the physically-adsorbed hydrogen. H_2-TPD profile was recorded in an Ar flowing at a heating rate of 10 °C/min from 50 to 700 °C. *In situ* FTIR was collected with a Bruker TENSOR II equipped with an MCT narrow-band detector.

1.4 Catalytic evaluations

The fatty acids hydrodeoxygenation reactions were carried out by using a stainless-steel batch reactor (25 mL). Take palmitic acid as an example: To begin, palmitic acid (0.1 g), dodecane (15 mL) and catalyst (0.03 g) were added into a 50 mL stainless-steel autoclave. Subsequently, the reactor underwent thorough purging with H_2 (>99.9%) at 1.0 MPa for five cycles before being pressurized and sealed with H_2 at 2.0 MPa. The reaction commenced at 240 ℃ under continuous stirring at 700 rpm. Liquid product identification and quantitative analysis were carried out using GC-MS (Agilent, 7890B GC/5977 A MS) and gas chromatograph spectrometer (Shimadzu GC-2014 C) furnished with a flame ionization detector. To test the stability of the catalyst, four to seven rounds of reactions were carried out. In each round of reactions, the catalyst was used directly after centrifugal separation and washed three times with ethanol without any other treatment.

The conversion and product selectivity were calculated according to the following equations:

$$\text{Conversion (\%)}=\frac{\text{Mol initial reactant-Mol unreacted reactant}}{\text{Mol initial reactant}}\times 100$$

$$\text{Selectivity (\%)}=\frac{\text{Mol amount of one product}}{\text{Mol total reactant converted in the liquid}}\times 100$$

1.5 Computational method

Spin-polarized periodic density functional theory (DFT) calculations were performed using Vienna Ab initio Simulation Package (VASP) 6.3.2,[1,2] with Perdew-Burke-Ernzerhof (PBE) functional in the generalized gradient approximation (GGA) describing the exchange-correlation

energies of the electrons.[3] The projected augmented wave (PAW) was used for approximate treatment of atom-electron interactions.[4,5] Γ-point sampling was adopted to describe the surface Brillouin zone. Additionally, the influence of van der Waals interaction was considered via Grimme's DFT-D3 method.[6] The plane-wave cutoff energy was set to 400 eV, and the convergence thresholds of energy and force were 1 × 10-4 eV and -0.02 eV/Å respectively. The Dimer method was employed to identify transition states.[7]

■ SUPPLEMENTARY DATA

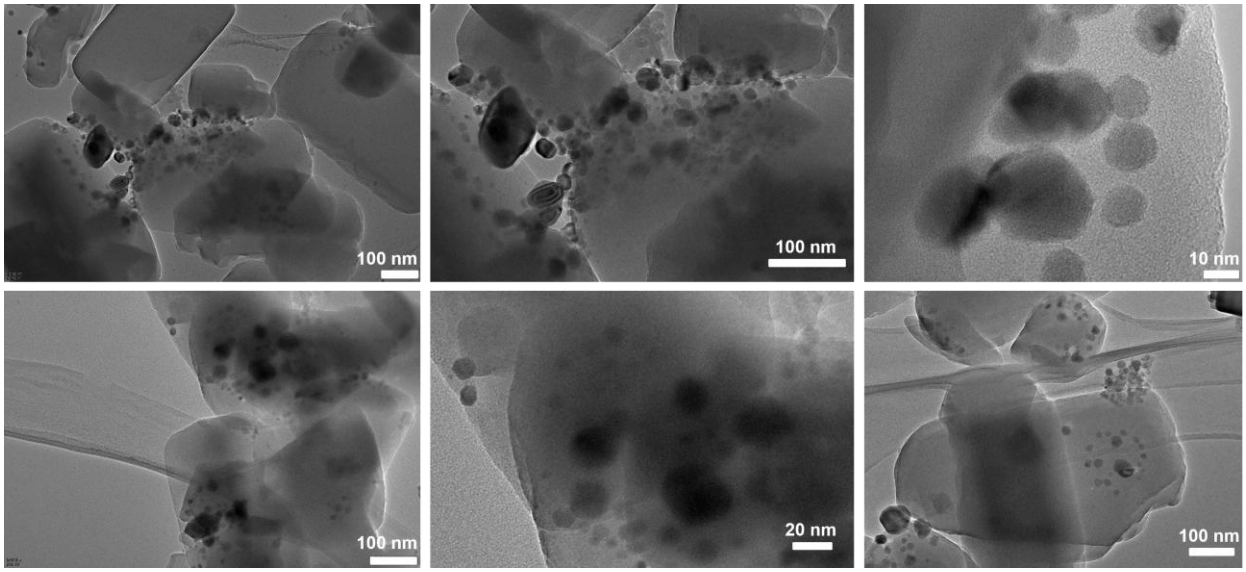

Figure S1. TEM image of the surface supported structure on Ni/ZSM-5 catalyst.

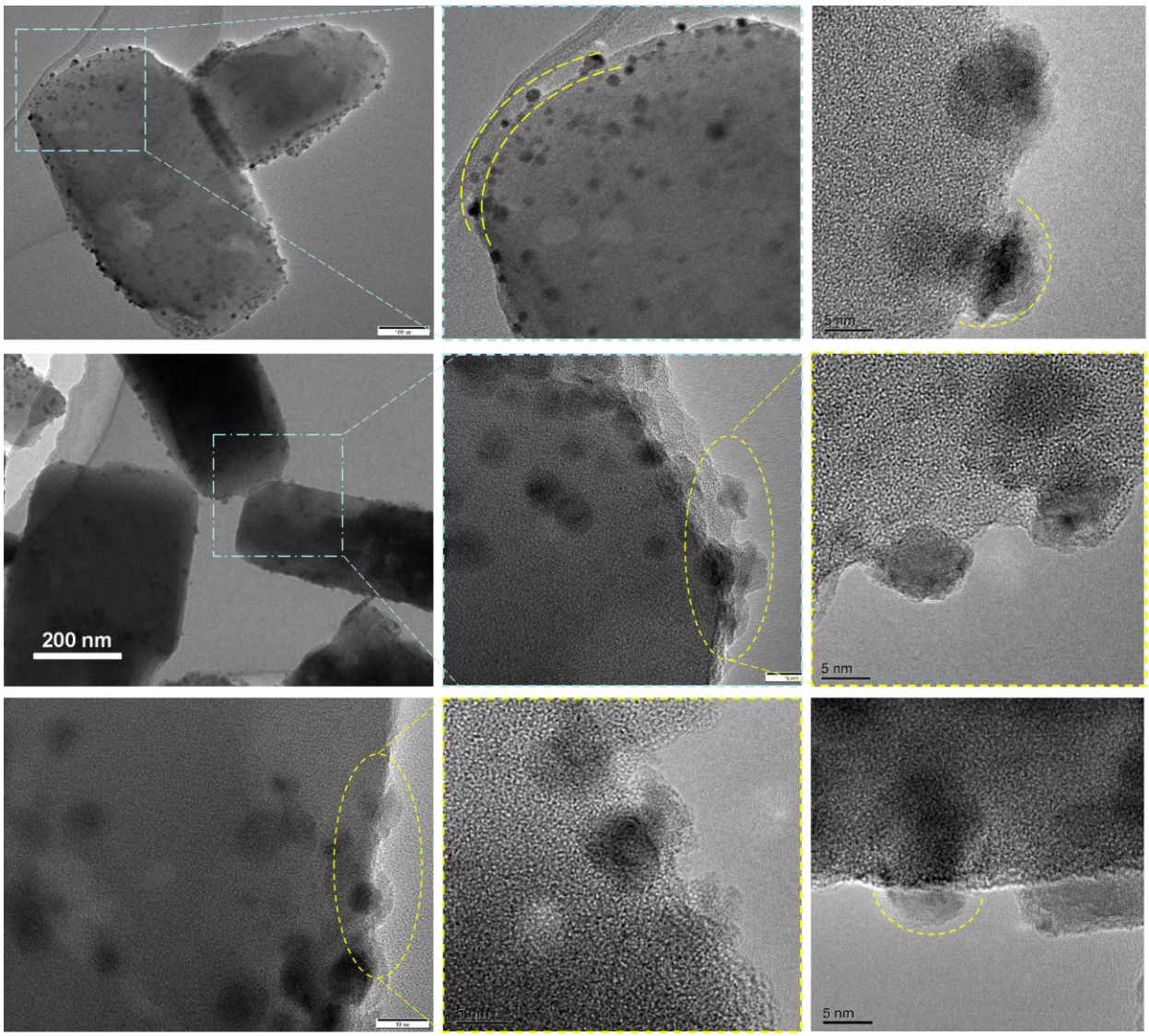

Figure S2. TEM image of the semi-embedded structure on Ni@ZSM-5 catalyst.

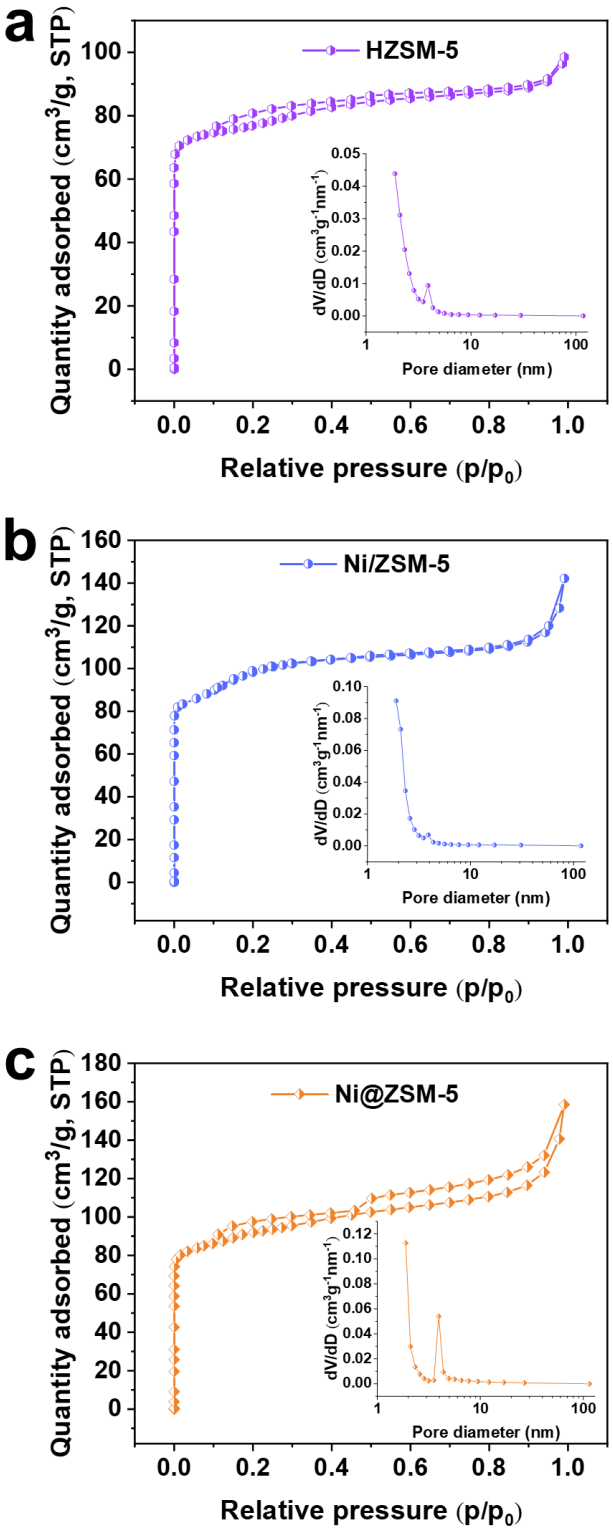

Figure S3. N_2 sorption isotherms and pore size distribution of (a) HZSM-5 support, (b) Ni/ZSM-5 catalyst, (c) Ni@ZSM-5 catalyst.

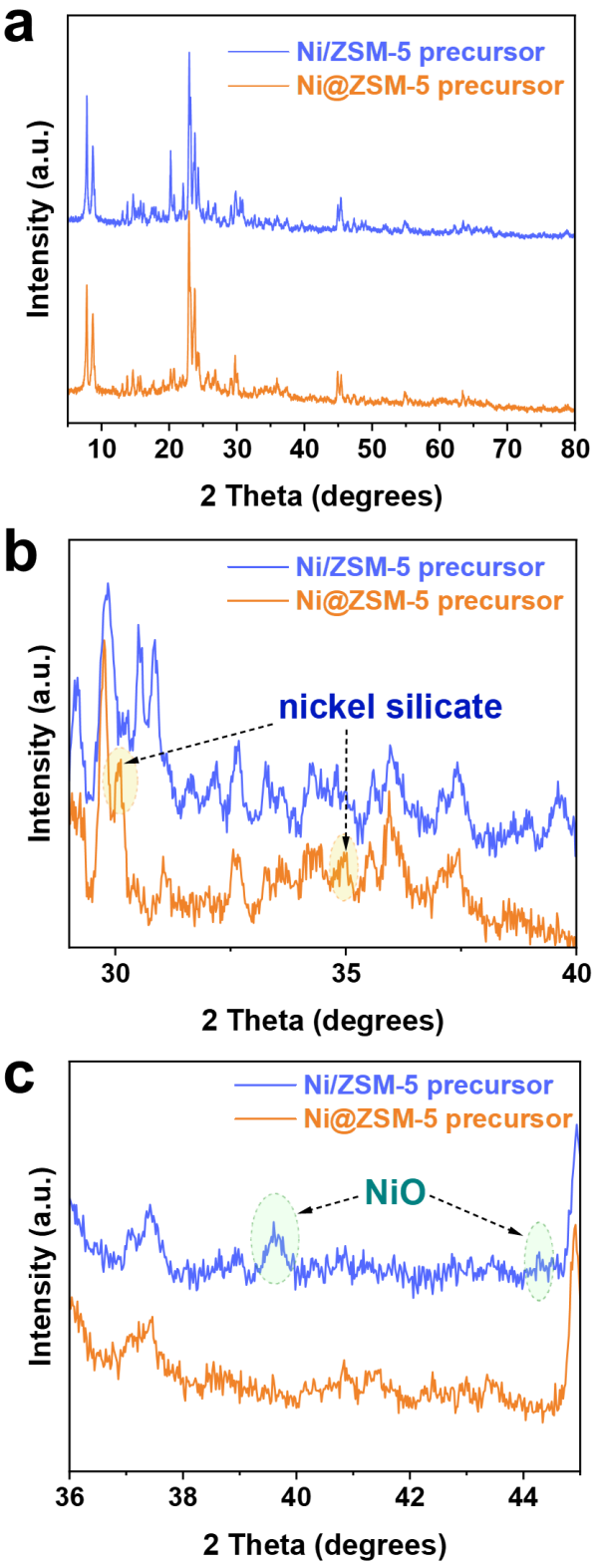

Figure S4. XRD patterns of (a) Ni/ZSM-5 and Ni@ZSM-5 precursors, (b) Locally magnified XRD patterns from 30 to 40 degrees, and (c) Locally magnified XRD patterns from 36 to 45 degrees.

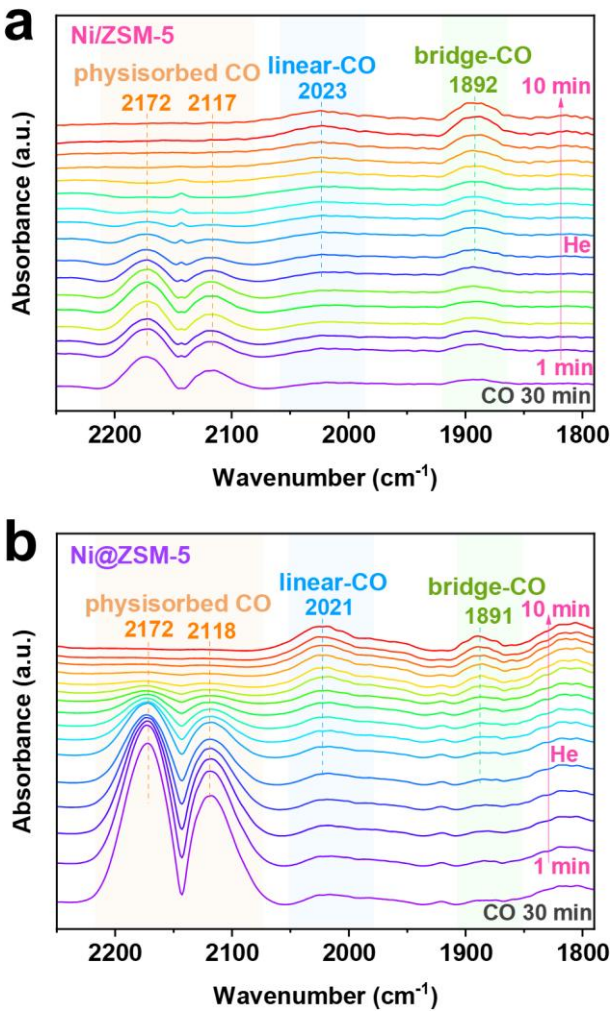

Figure S5. *In situ* FT-IR spectra of CO adsorption on (a) Ni/ZSM-5 catalyst, and (b) Ni@ZSM-5 catalyst.

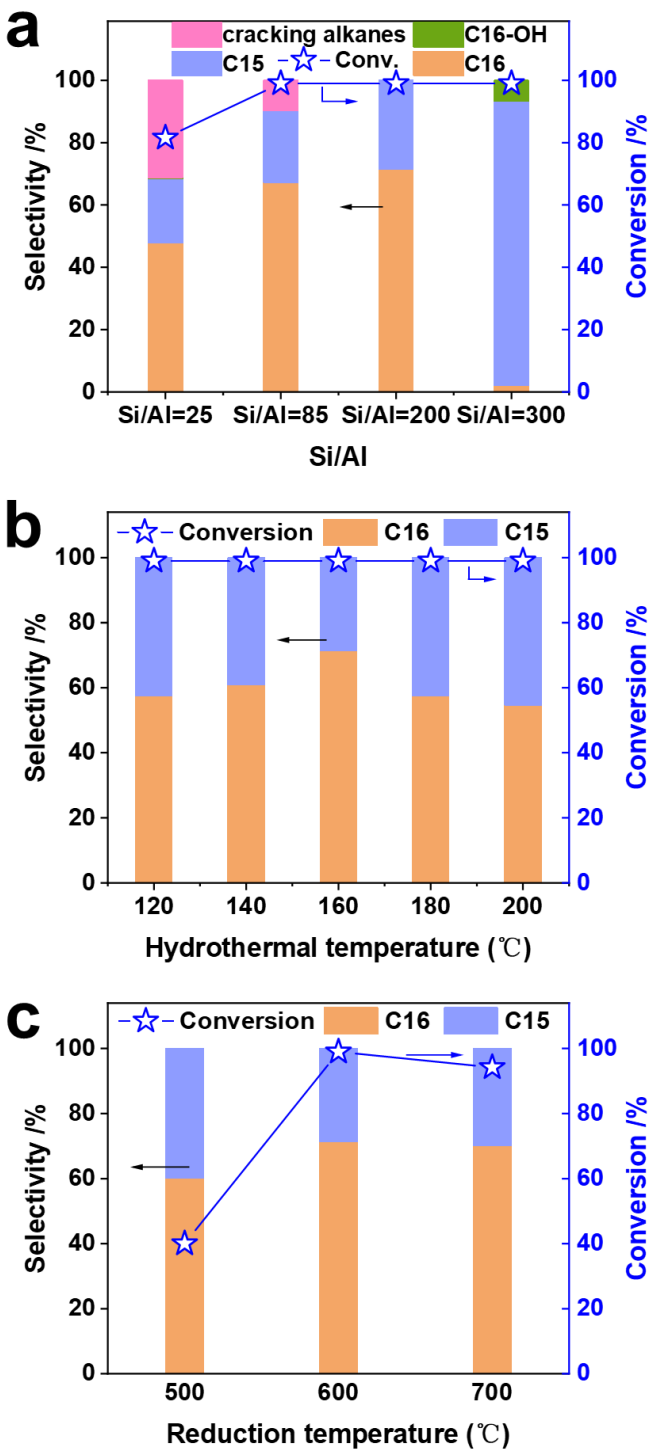

Figure S6. Screening of catalyst synthesis conditions: (a) The effect of Si/Al ratio, (b) The effect of hydrothermal temperature, (c) The effect of reduction temperature.

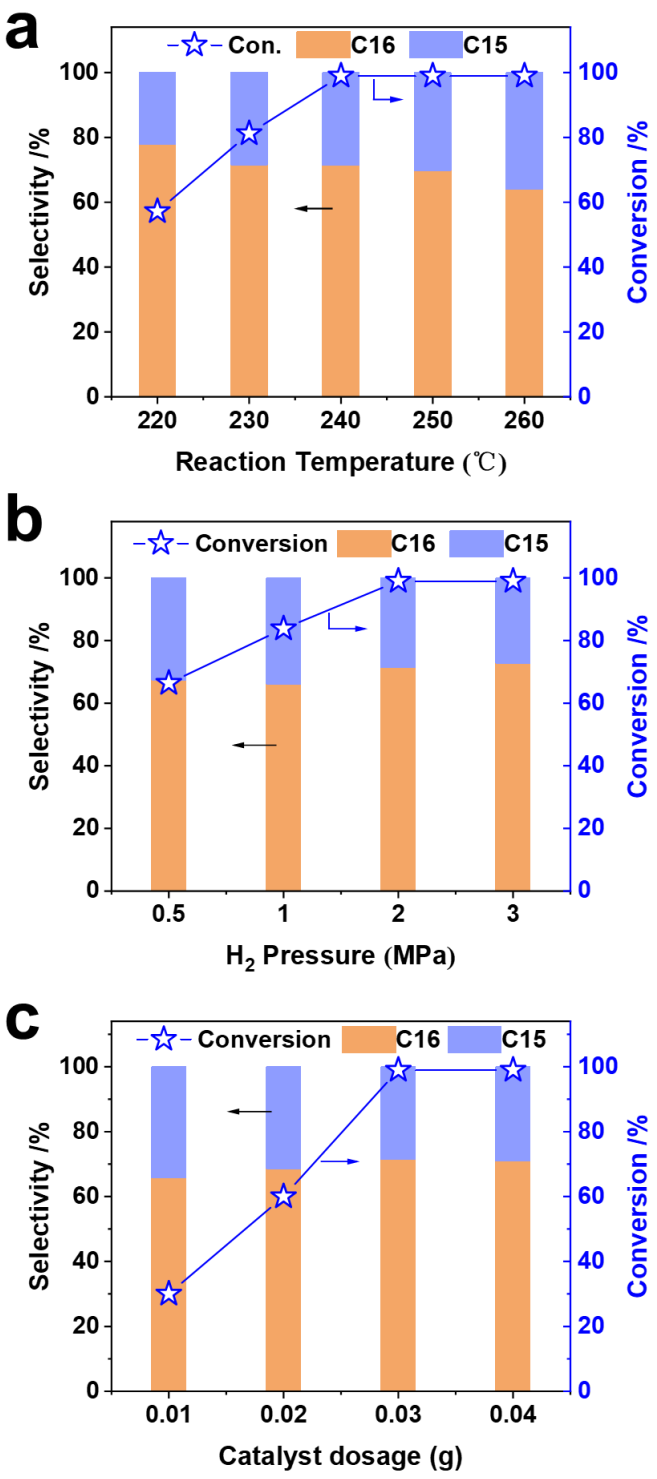

Figure S7. Optimization of the reaction conditions of Ni@ZSM-5 catalyst: (a) The effect of reaction temperature, (b) The effect of H_2 pressure, (c) The effect of catalyst dosage.

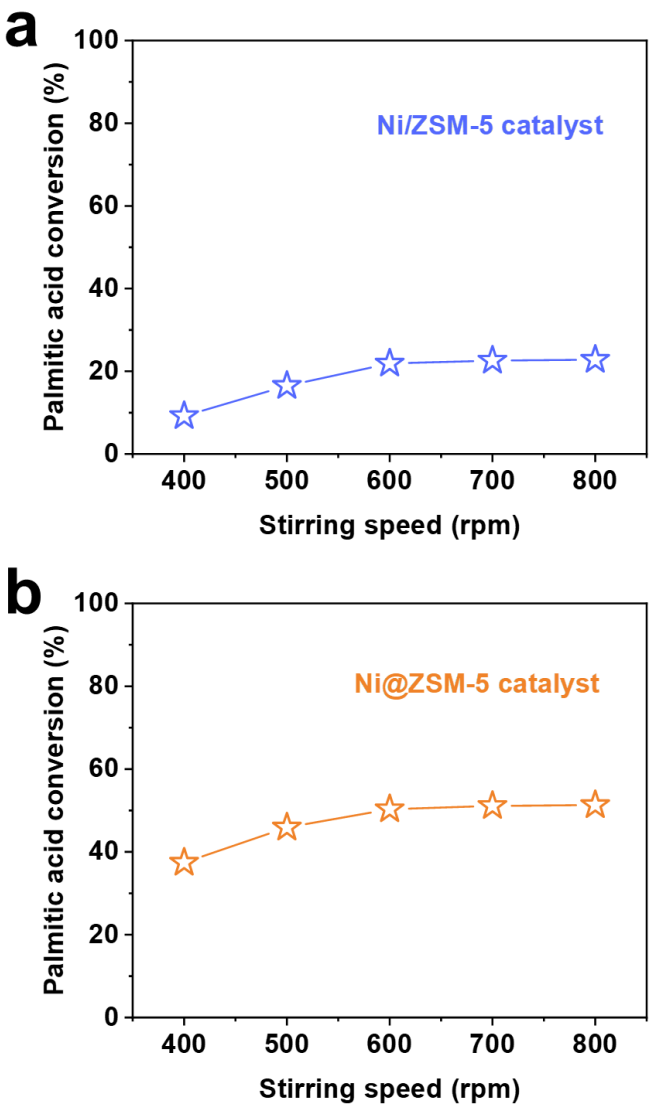

Figure S8. Effect of stirring speed on the conversion of palmitic acid: (a) Ni/ZSM-5 catalyst, and (b) Ni@ZSM-5 catalyst. Reaction conditions: 240 °C, 2 MPa H_2, 0.1 g of substrate, 15 mL of dodecane, 0.03 g of catalyst, 1 h.

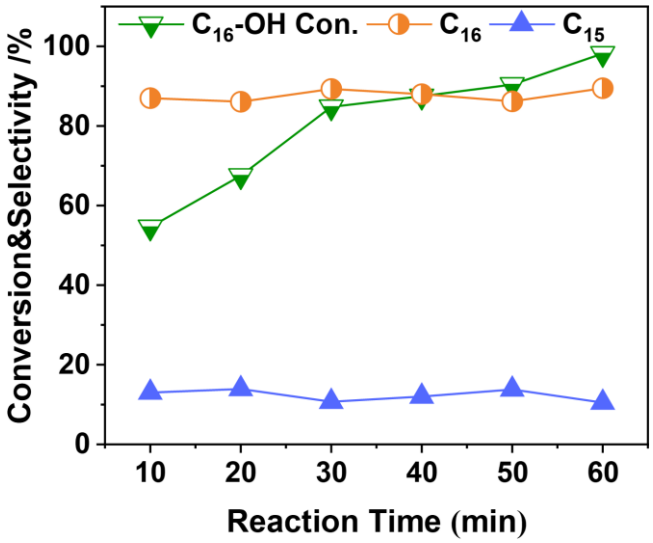

Figure S9. Time conversion curve of hexadecanol hydrodeoxygenation over Ni@ZSM-5. Reaction conditions: 240 °C, 2 MPa H_2, 0.1 g of hexadecanol, 0.03 g of catalyst, 15 mL of dodecane.

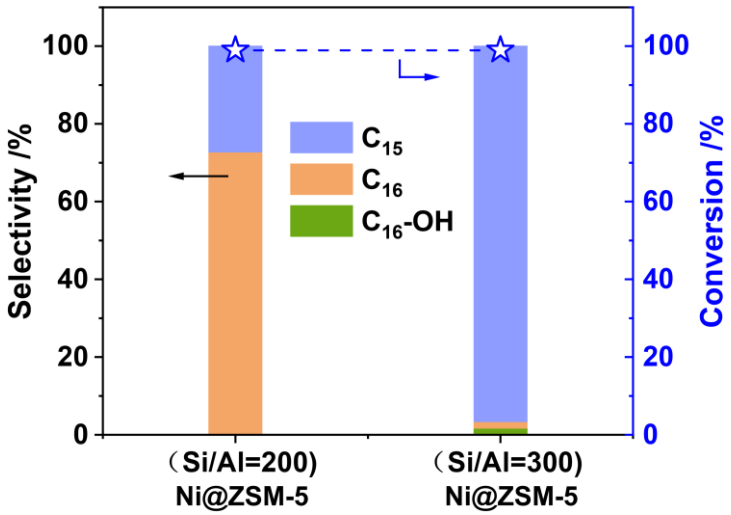

Figure S10. Hexadecanal deoxygenation reaction in the presence of Ni@ZSM-5 (Si/Al=200) and Ni@ZSM-5 (Si/Al=300) catalysts. Reaction conditions: 240 °C, 2 MPa H_2, 0.1 g of substrate, 0.03 g of catalyst, 15 mL of dodecane, 4 h.

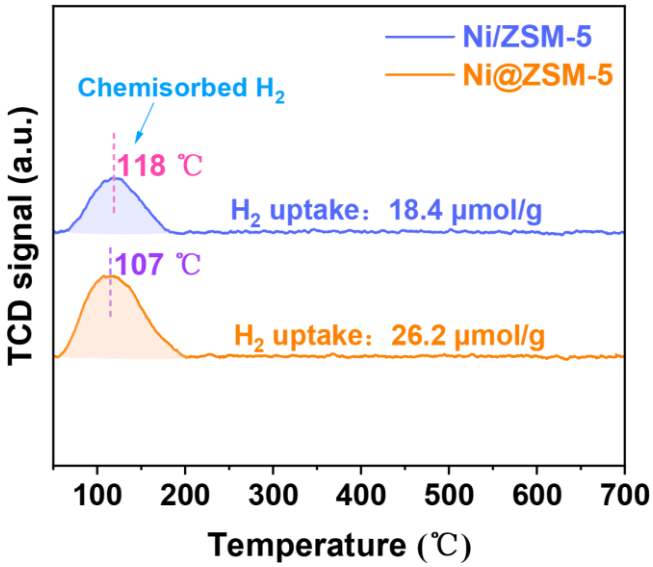

Figure S11. H_2-TPD profiles of the Ni/ZSM-5 and Ni@ZSM-5, respectively.

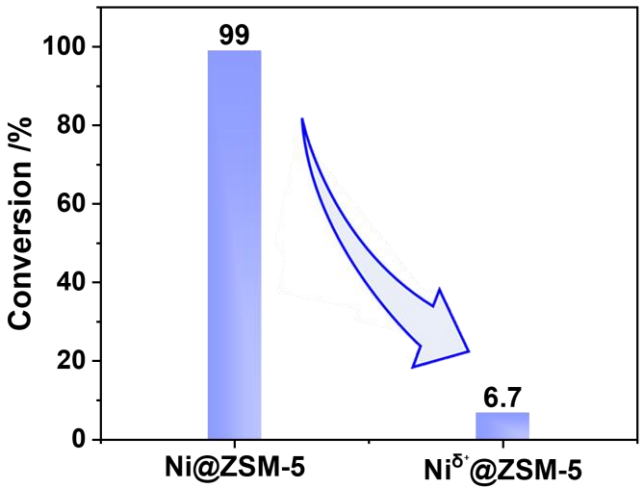

Figure S12. Palmitic acid deoxygenation reaction in the presence of Ni@ZSM-5 and $Ni^{\delta+}$@ZSM-5 catalysts. Reaction conditions: 240 °C, 2 MPa H_2, 0.1 g of substrate, 0.03 g of catalyst, 15 mL of dodecane, 4 h.

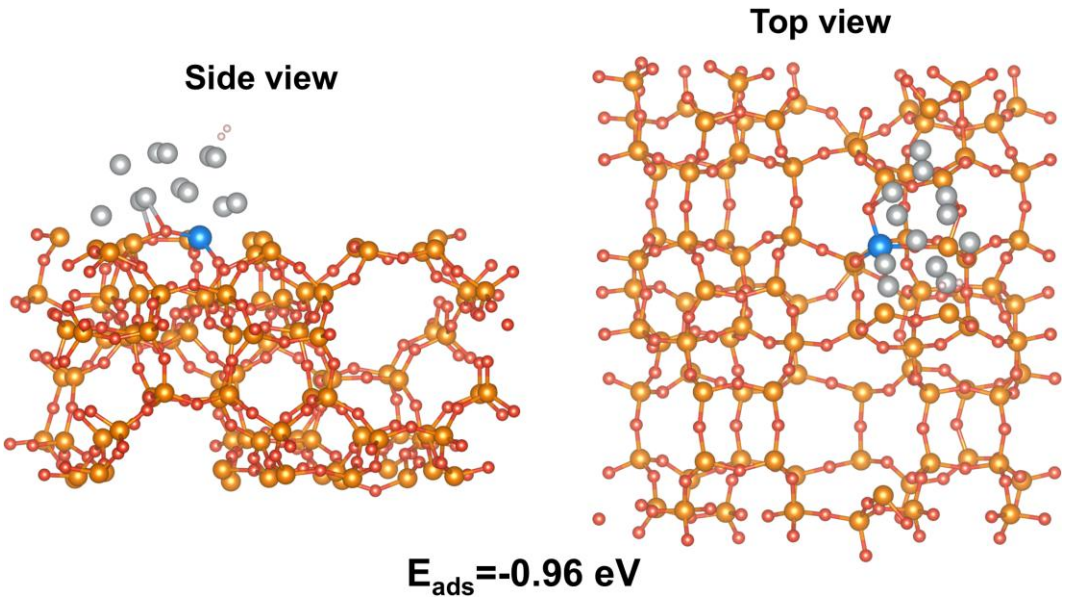

Figure S13. Adsorption energy of H_2 molecule on Ni@ZSM-5 model surface.

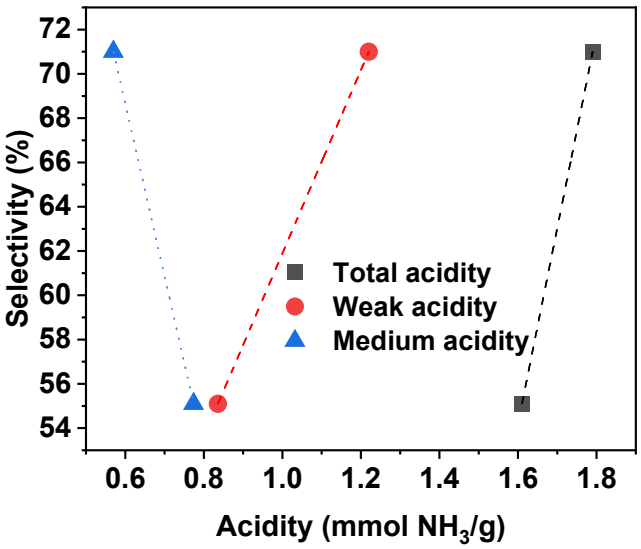

Figure S14. Correlation between weak/medium/total acid contents and C_{16} selectivity.

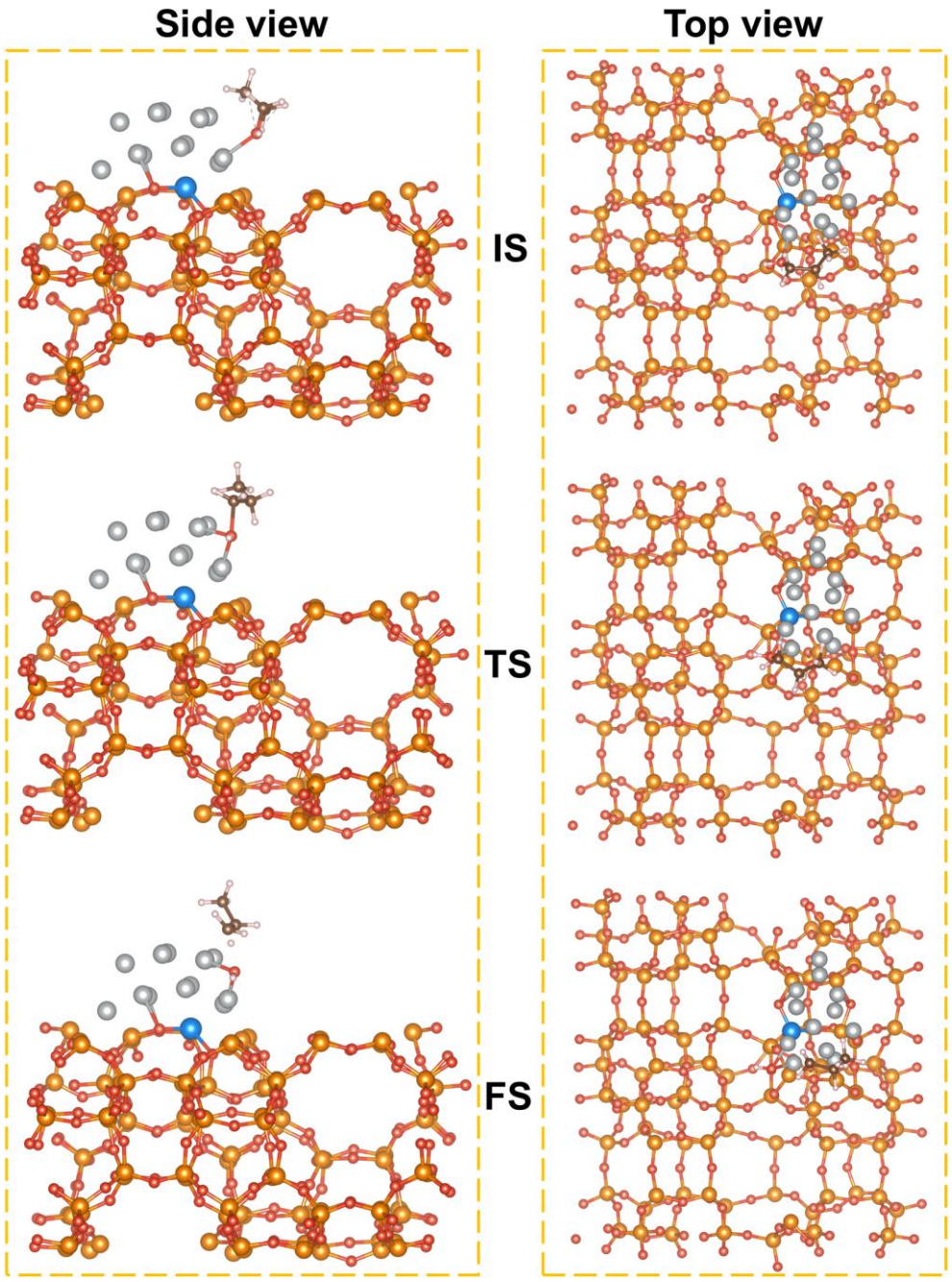

Figure S15. Optimized structures (Side and Top Views) of reaction intermediates and final states (FS) on Ni@ZSM-5 catalyst from DFT calculations, in which the orange, blue, white, gray and red represent Si, Al, H, C and O, respectively.

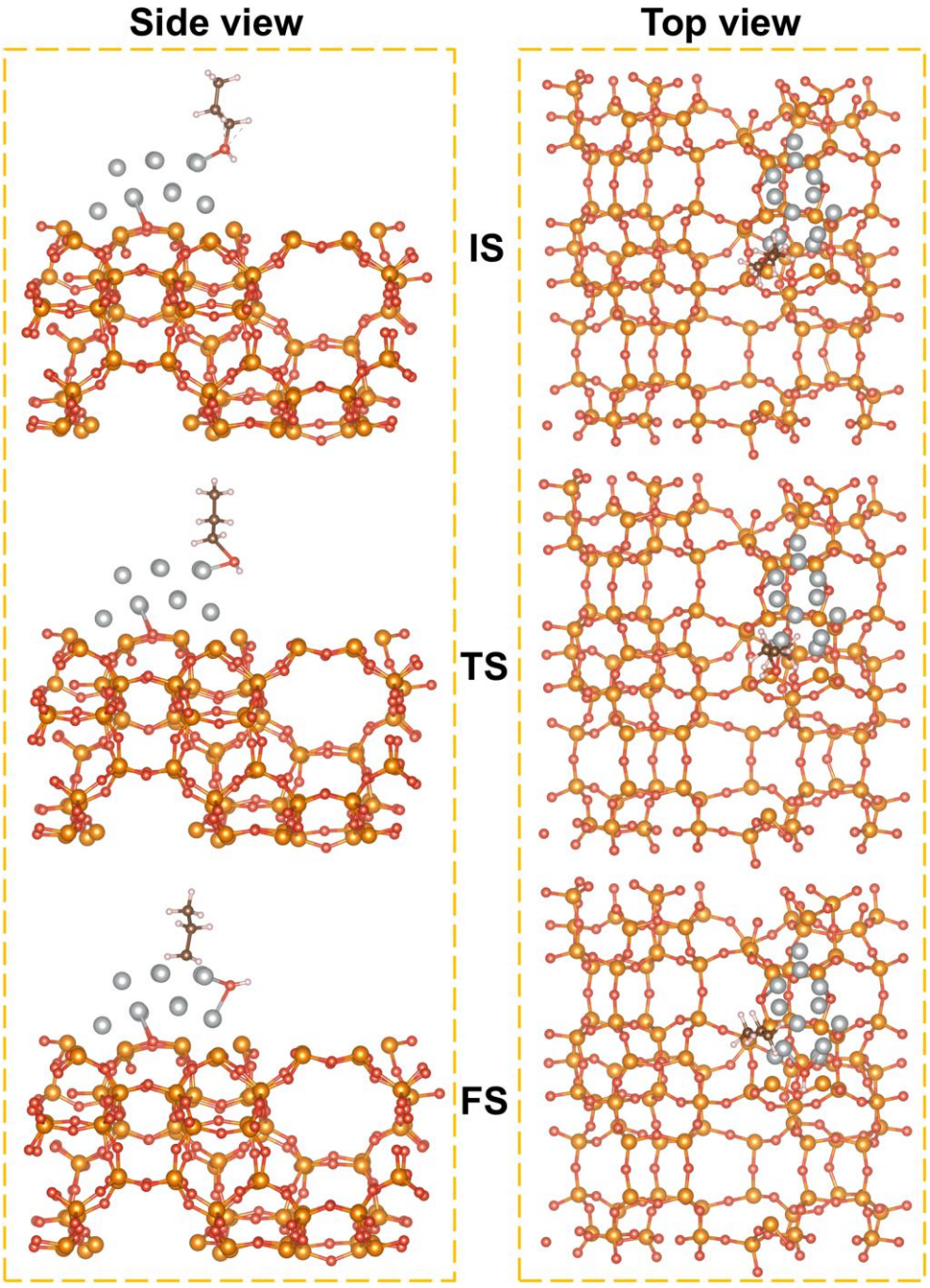

Figure S16. Optimized structures (Side and Top Views) of reaction intermediates and final states (FS) on pyridine-poisoned Ni@ZSM-5 catalyst from DFT calculations, in which the orange, blue, white, gray and red represent Si, Al, H, C and O, respectively.

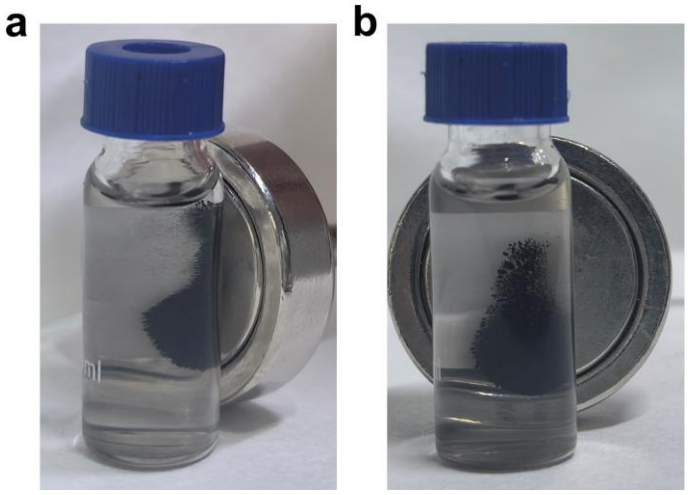

Figure S17. Magnetic recyclability test of the catalyst: (a) Ni@ZSM-5 catalyst, and (b) Ni/ZSM-5 catalyst.

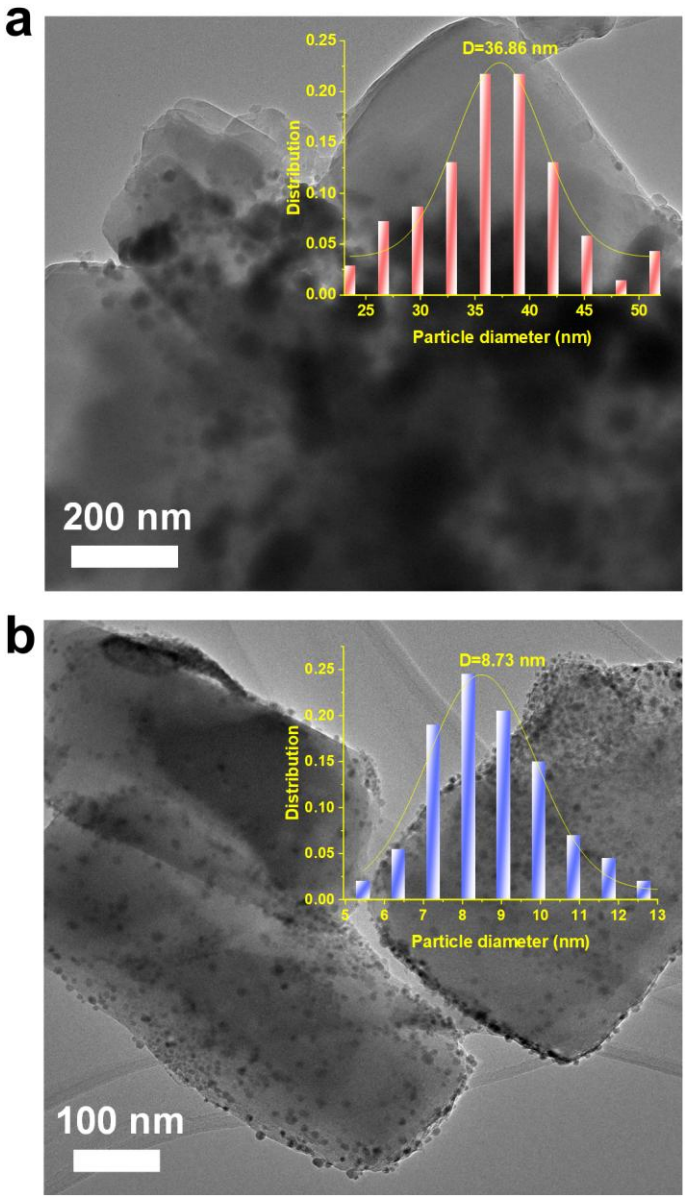

Figure S18. TEM images of (a) Used Ni/ZSM-5, (b) Used Ni@ZSM-5.

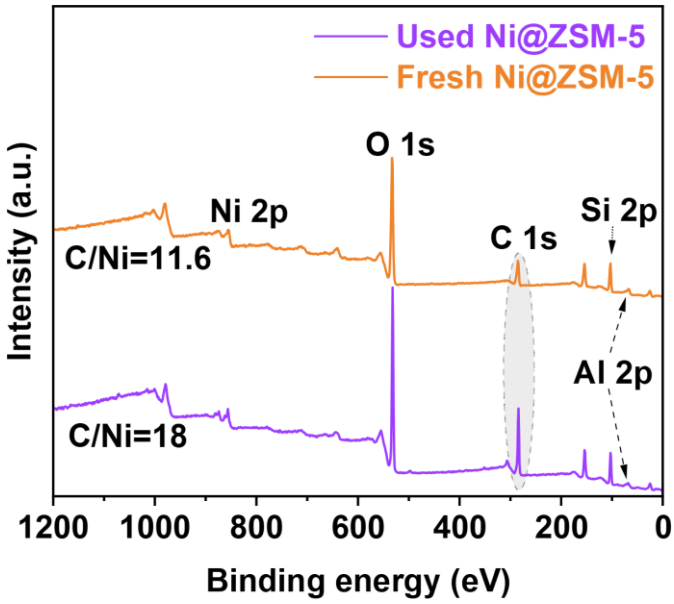

Figure S19. XPS survey spectra of fresh Ni@ZSM-5 and used Ni@ZSM-5.

Table S1. Physicochemical properties of the samples

Sample	S_{BET}[a] (m^2/g)	V_{Pore}[a] (cm^3/g)	$D_{Average}$[a] (nm)	Ni content (*wt.*%)[b]	Ni species (%)[c]	
					Ni^0	$Ni^{\delta+}$
HZSM-5	304.04	0.15	2.00	-	-	-
Ni/ZSM-5	355.29	0.22	2.46	9.9 (fresh) 9.2 (used)	41.5	48.5
Ni@ZSM-5	346.04	0.24	2.82	9.8 (fresh) 9.6 (used)	32.4	67.6

[a] Values determined by BET method. [b] Values determined by ICP-AES. [c] Values determined by XPS.

Table S2. Curve-fitting results of Ni K-edge EXAFS spectra for Ni@ZSM-5 and Ni/ZSM-5 samples

Sample	Shell	R (Å)[a]	CN[b]	σ^2 (10^{-3} Å^2)[c]	ΔE_0 (eV)[d]	R factor (%)[e]
Ni@ZSM-5	Ni–O	2.02	2.1 (0.9)	6.4	7.02	1.4
	Ni–Ni	2.48	6.8 (0.6)	5.7	6.32	
	Ni–O–(Ni/Si)	2.99	2.5 (0.5)	8.0	9.80	
Ni/ZSM-5	Ni–Ni	2.48	10.5 (1.0)	5.9	7.11	1.4
Ni-foil	Ni–Ni	2.48	12.0	5.6	6.36	0.5

[a] R: bond distance; [b] CN: coordination number; [c] σ^2: Debye-Waller factor; [d] ΔE_0: the inner potential correction. The accuracies of the above parameters were estimated as follows: CN, ±20%; R, ±1%; σ^2, ±20%; ΔE_0, ± 20%. The data ranges used for data fitting in k space (Δk) and R space (ΔR) are 2.0−12.0 Å^{-1} and 1.0−3.0 Å, respectively.

Table S3. Catalytic performance of Ni@ZSM-5 in this work comapared with reported studies

Catalyst/ (substrate)	Reaction conditions	Conv. (%)	C_n+C_{n-1} Sel.(%)	C_n/C_{n-1}	Reuse times	TOF (h^{-1})	Refer.
Ni@ZSM-5 (palmitic acid)	240 °C, 2 MPa H_2, 4 h Rea/Cat (wt/wt)=3.3 Rea/Sol (g/ml)=0.007	99	99	2.5	7	26.6 [a] 3.85 [b]	This work
Co@CN–900 (palmitic acid)	280 °C, 4 MPa H_2, 5 h Rea/Cat (wt/wt)=2 Rea/Sol (g/ml)=0.01	99	91.7	1.4	7	1.31 [b]	[8]
Ni/H–CeO_2 (palmitic acid)	270 °C, 2 MPa H_2, 10 h Rea/Cat (wt/wt)=5 Rea/Sol (g/ml)=0.01	99	94.8	0	3	23.5 [a]	[9]
Ni_3Mo_3N@600 (palmitic acid)	270 °C, 2 MPa H_2, 10 h Rea/Cat (wt/wt)=10 Rea/Sol (g/ml)=0.01	99	94.3	4.4	5	1.37 [b]	[10]
Pd@Al_x–mSiO_2 (palmitic acid)	260 °C, 3 MPa H_2, 5 h Rea/Cat (wt/wt)=3.3 Rea/Sol (g/ml)=0.01	98	99	2.5	5	-	[11]
$Ni_{0.5}$@$C_{0.5}$ (palmitic acid)	280 °C, 4 MPa H_2, 2 h Rea/Cat (wt/wt)=2 Rea/Sol (g/ml)=0.01	99	97.9	0.15	6	4.74 [a]	[12]
7% Ni/RM (palmitic acid)	300 °C, 4 MPa H_2, 4 h Rea/Cat (wt/wt)=5 Rea/Sol (g/ml)=0.01	99	99	0.4	3	-	[13]
Mo-Ni@Al_2O_3 (palmitic acid)	230 °C, 3 MPa H_2, 5 h Rea/Cat (wt/wt)=3.3 Rea/Sol (g/ml)=0.01	99	96.3	3.2	4	11.4 [a]	[14]
Ni/$Ti_3C_2T_x$ (palmitic acid)	300 °C, 4 MPa H_2, 4 h Rea/Cat (wt/wt)=5 Rea/Sol (g/ml)=0.01	99	78.1	0.38	5	26.6 [a]	[15]
Ni/CeO_2–r (palmitic acid)	300 °C, 4 MPa H_2, 3 h Rea/Cat (wt/wt)=2 Rea/Sol (g/ml)=0.01	98.9	92.4	0.9	2	41.5 [a]	[16]
Co@SiO_2 (palmitic acid)	300 °C, 2 MPa H_2, 4 h Rea/Cat (wt/wt)=3 Rea/Sol (g/ml)=0.01	99	96.3	4.6	4	0.38 [b]	[17]

Ni/AC-KP (palmitic acid)	260 °C, 4 MPa H_2, 3 h Rea/Cat (wt/wt)=2 Rea/Sol (g/ml)=0.01	96.2	86.5	0.03	2	2.3 [a]	[18]
Ni/AC–H (palmitic acid)	280 °C, 4 MPa H_2, 8 h Rea/Cat (wt/wt)=2 Rea/Sol (g/ml)=0.01	100	99.3	0.05	1	6.6 [a]	[19]
Ni-Mo/RM (palmitic acid)	325 °C, 4 MPa H_2, 4 h Rea/Cat (wt/wt)=5 Rea/Sol (g/ml)=0.01	99	99	3.06	-	-	[20]
ReNi/M-TiO_2-S (lauric acid)	190 °C, 4 MPa H_2, 6 h Rea/Cat (wt/wt)=5 Rea/Sol (g/ml)=0.02	100	100	2.03	3	24.9 [a]	[21]
Ni/$NiAl_2O_4$@mSiO_2 (stearic acid)	250 °C, 3 MPa H_2, 4 h Rea/Cat (wt/wt)=1.75 Rea/Sol (g/ml)=0.028	99	97.6	0.04	4	3.36 [b]	[22]
NiCu/10%Mo– $NbOPO_4$ (oleic acid)	250 °C, 3 MPa H_2, 7 h Rea/Cat (wt/wt)=5 Rea/Sol (g/ml)=0.1	99.6	94.6	8.04	5	1.7 [b]	[23]
Ni/Co-S (stearic acid)	290 °C, 4 MPa H_2, 3 h Rea/Cat (wt/wt)=0.6 Rea/Sol (g/ml)=0.01	99	90.1	14.08	-	8.97 [a]	[24]
NiCo/SiO_2 (stearic acid)	280 °C, 1 MPa H_2, 3 h Rea/Cat (wt/wt)=1.67 Rea/Sol (g/ml)=0.025	83	84	mainly C_{n-1}	-	1.19 [b]	[25]
7Ni/SAPO-11 (oleic acid)	360 °C, 4 MPa H_2, 4 h Rea/Cat (wt/wt)=21.4 Rea/Sol (g/ml)=0.1	95.3	75.7	0.83	5	82.6 [a]	[26]
Ru/HZSM-5 (stearic acid)	260 °C, 3 MPa H_2, 5 h Rea/Cat (wt/wt)=1.33 Rea/Sol (g/ml)=0.02	100	87.4	1.01	4	7.73 [a]	[27]

[a] TOF value calculated based on the active metal sites: TOF (h^{-1}) = (C_n+C_{n-1} alkanes formed (mmol))/(surface atoms of active metal (mmol))(reaction time (h)).

[b] TOF value calculated based on total metal amount: TOF (h^{-1}) = (C_n+C_{n-1} alkanes formed (mmol))/(total metal amount (mmol))(reaction time (h)).

Table S4. Hydrodeoxygenation of various fatty acid substrates over Ni@ZSM-5

Entry	Substrate	Conv. (%)	C_n product	C_n Sel. (%)	C_{n-1} product	C_{n-1} Sel. (%)
1[a]	Palmitic acid	99	$C_{16}H_{34}$	71.0	$C_{15}H_{32}$	28
2[a]	Oleic acid	99	$C_{18}H_{38}$	70.2	$C_{17}H_{36}$	28.8
3[a]	Stearic acid	99	$C_{18}H_{38}$	69.7	$C_{17}H_{36}$	29.3
4[a]	Myristic acid	99	$C_{14}H_{30}$	72.2	$C_{13}H_{28}$	26.8
5[a]	Lauric acid	99	$C_{12}H_{26}$	72.6	$C_{11}H_{24}$	26.4
6[b]	Methyl palmitate	98	$C_{16}H_{34}$	69.4	$C_{15}H_{32}$	29.6
7[b]	Methyl stearate	98	$C_{18}H_{38}$	70.3	$C_{17}H_{36}$	28.7
8[b]	Methyl laurate	99	$C_{12}H_{26}$	71.8	$C_{11}H_{24}$	27.2

[a] Reaction conditions: 240 °C, 2 MPa H_2, 0.1 g of substrate, 0.03 g of catalyst, 15 mL of solvent, 4 h.

[b] Reaction conditions: 240 °C, 2 MPa H_2, 0.1 g of substrate, 0.03 g of catalyst, 15 mL of solvent, 6 h.

REFERENCES

[1] G. Kresse and J. Furthmüller, *Comput. Mater. Sci.*, 1996, **6**, 15–50.

[2] G. Kresse and J. Furthmüller, *Phys. Rev. B*, 1996, **54**, 11169–11186.

[3] B. Hammer, L. B. Hansen and J. K. Nørskov, *Phys. Rev. B*, 1999, **59**, 7413.

[4] G. Kresse and D. Joubert, *Phys. Rev. B*, 1999, **59**, 1758–1775.

[5] P. E. Blöchl, *Phys. Rev. B*, 1994, **50**, 17953–17979.

[6] S. Grimme, J. Antony, S. Ehrlich and H. Krieg, *J. Chem. Phys.*, 2010, **132**, 154104.

[7] G. Henkelman and H. Jónsson, *J. Chem. Phys.*, 1999, **111**, 7010–7022.

[8] M. Lin, D. Jiang, Y. Yan, X. Li, L. Zhan, X. Song, R. Li and Y. Wu, *Chem. Eng. J.*, 2024, **481**, 148565.

[9] Z. Yan, H. Wang, H. Yang, C. Juan, D. Li, X. Wen, F. Zhang, J.-J. Zou, C. Peng and C. Hu, *Chin. J. Catal.*, 2023, **47**, 229–242.

[10] X. Du, X. Lei, L. Zhou, Y. Peng, Y. Zeng, H. Yang, D. Li, C. Hu and H. Garcia, *ACS Catal.*, 2022, **12**, 4333–4343.

[11] X. Cao, J. Zhao, F. Long, X. Zhang, J. Xu and J. Jiang, *Appl. Catal. B: Environ.*, 2022, **305**, 121068.

[12] M. Lin, X. Li, Y. Yan, R. Li and Y. Wu, *Chem. Eng. J.*, 2023, **471**, 144336.

[13] J. Chen, D. Wang, F. Luo, X. Yang, X. Li, S. Li, Y. Ye, D. Wang and Z. Zheng, *Fuel*, 2022, **314**, 122780.

[14] X. Cao, S. Wu, J. Zhao, F. Long, S. Jia, X. Zhang, J. Xu and J. Jiang, *Appl. Catal. B: Environ.*, 2024, **343**, 123506.

[15] J. Liang, Q. Zhang, H. Zhao, S. Zhao, Y. Wu and X. Fan, *Ind. Eng. Chem. Res.*, 2022, **61**, 13275–13282.

[16] M. Lin, Y. Yan, D. Jiang, X. Li, R. Li and Y. Wu, *Chem. Eng. J.*, 2023, **475**, 146357.

[17] M. Lin, X. Zhang, L. Zhan, X. Li, X. Song and Y. Wu, *Fuel*, 2022, **318**, 123605.

[18] M. Lin, Y. Yan, X. Li, R. Li and Y. Wu, *Fuel Process. Technol.*, 2023, **250**, 107892.

[19] M. Lin, Y. Yan, X. Li, R. Li and Y. Wu, *Chin. J. Chem. Eng.*, 2024, **66**, 8–18.

[20] Q. Wang, X. Li, J. Duan, J. Chen, Y. Ye, D. Wang, S. Li and Z. Zheng, *Fuel*, 2022, **329**, 125447.

[21] P. Huang, Z. Lv, J. Zhang, T. Niu, Y. Leng, M. Fan and P. Zhang, *Fuel*, 2025, **379**, 133031.

[22] X. Zhao, J. Yang, B. Chen, B. Li, J. A. Wang, R. Nie, J. Fu and C. C. Xu, *Energy Fuels*, 2025, **39**, 22534–22542.

[23] R. Wei, L. Zhang, M. Tian, Z. Cai, Z. Shao, L. Gao, J. Zhang, X. Guo and G. Xiao, *New J. Chem.*, 2025, **49**, 4849–4859.

[24] D. Zheng, D. Guo, Z. Wang, X. Wang, Y. Shan, X. Liu, Z. Yan, S. Yu and Y. Liu, *Chem. Eng. J.*, 2023, **451**, 138929.

[25] H. Lin, Y. Chu, M. Xie, L. Yang and G. Ouyang, *J. Environ. Chem. Eng.*, 2023, **11**, 110825.

[26] L. Yang, S. Xing, H. Sun, C. Miao, M. Li, P. Lv, Z. Wang and Z. Yuan, *Fuel Process. Technol.*, 2019, **187**, 52–62.

[27] J. Chen and Q. Xu, *Catal. Sci. Technol.*, 2016, **6**, 7239–7251.

The following section is the results of GC and GC-MS:

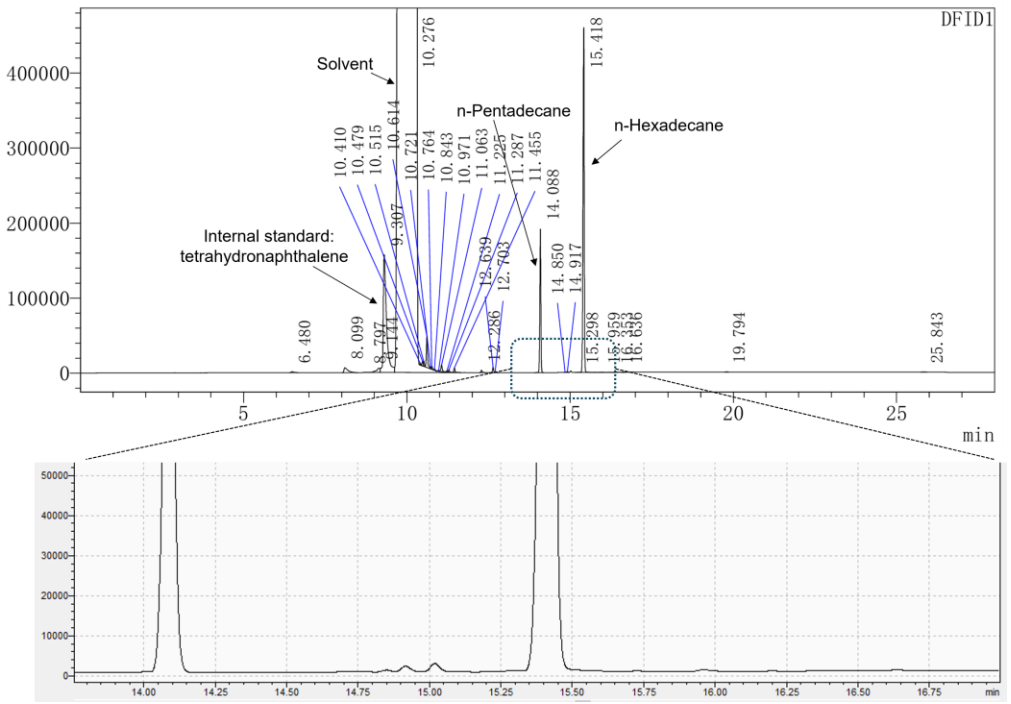

Note: In each experiment, the selectivity for pentadecane and hexadecane exceeded 99%, while the combined contribution of isomeric alkanes and trace impurities originating from the reactants, solvent, or the GC system remained below 1%.

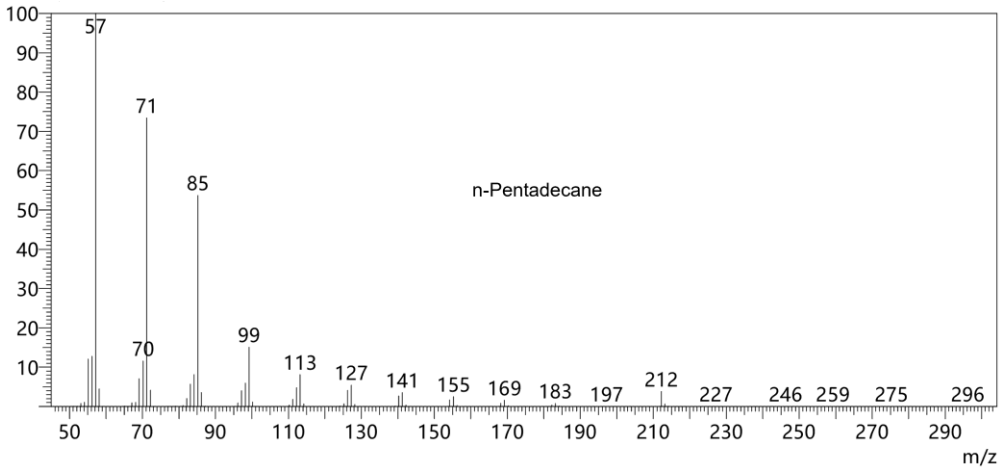

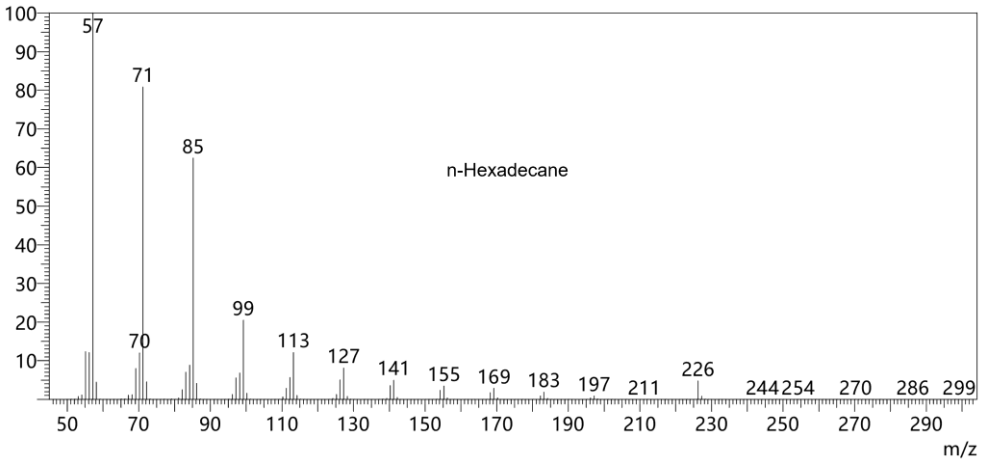
n-Hexadecane
57
71
85
99
70
113
127
141
155
169
183
197
211
226
244
254
270
286
299
m/z